

## THE PROPER MOTION OF THE SOFT X-RAY-EMITTING RADIO PULSAR PSR 0656 + 14

R. J. THOMPSON, JR.<sup>1</sup> AND F. A. CORDOVA<sup>1</sup>

Department of Astronomy and Astrophysics, 525 Davey Laboratory, The Pennsylvania State University, University Park, PA 16802

R. M. HJELLMING

National Radio Astronomy Observatory,<sup>2</sup> P.O. Box O, Socorro, NM 87801

AND

E. B. FOMALONT

National Radio Astronomy Observatory, Edgemont Road, Charlottesville, VA 22901

Received 1990 September 4; accepted 1990 October 24

### ABSTRACT

Using the Very Large Array, we have measured the motion of the soft X-ray-emitting radio pulsar PSR 0656 + 14 relative to background radio sources. From observations at epochs 1989.07 and 1990.38, we have determined its proper motion to be  $0''.078 \pm 0''.012$  at position angle  $294^\circ$ . For an assumed distance of 300 pc, the pulsar has a transverse velocity of  $\sim 115 \text{ km s}^{-1}$ . PSR 0656 + 14, as noted by Nousek and coworkers, is very close to the geometric center of a  $20^\circ$  diameter ring of soft X-ray emission. Previous work has shown that the ages and distances of the pulsar and the ring are similar. The present measurement, which shows that the direction of the pulsar's motion is away from the center of the ring, strengthens the contention that the ring of soft X-ray emission is the 100,000 year old supernova remnant of the pulsar's progenitor.

*Subject headings:* nebulae: supernova remnants — pulsars — stars: individual (PSR 0656 + 14) — stars: neutron — stars: proper-motion — stars: radio radiation — X-rays: sources

### 1. ASTROMETRY

We have made two observations of the radio pulsar PSR 0656 + 14 using the A-array of the VLA. These observations were made at a frequency of 1.385 GHz, in the VLA's spectral line mode (16 channels with a total bandwidth of 50 MHz). Since radial smearing is proportional to bandwidth and the distance of the source from the center of the field, spectral line mode was used to constrain this smearing to an acceptable level. The observations were each 5 hr in duration; the images used for position fitting had an rms noise of  $\sim 0.05 \text{ mJy}$ . This allowed us to reach a signal-to-noise ratio of  $\sim 90:1$  for the pulsar and much higher for the other sources in the field. The observations took place on 1989 January 25 and 1990 May 19, a difference of 1.3 yr.

The data were edited and calibrated using the NRAO Astronomical Image Processing System (AIPS). The calibration sources observed were 3C 48 and 0622 + 147. The flux density scale was based on 16.6 Jy for 3C 48, and all positions were tied to that of 0622 + 147, which we assume has a right ascension of  $06^{\text{h}}22^{\text{m}}54^{\text{s}}.77$  and a declination of  $+14^\circ42'06''.00$ . Since the VLA analysis software does not correct the effects of yearly aberration with sufficient accuracy, a relative rotation between images is produced. This rotation was corrected through the use of the AIPS task UVFIX.

The AIPS task MX was then used to create a "dirty" image of the entire field of view which was centered on coordinates  $\alpha = 06^{\text{h}}56^{\text{m}}57^{\text{s}}.5$ ,  $\delta = +14^\circ17'0''.00$ ,  $1'.57$  south and west of the pulsar, to include as many background sources as possible. The first step of the analysis process was to create a low-

resolution image of the field of view in order to find the bright background sources near the pulsar. This low-resolution image is shown in Figure 1. Ten background sources (constituting all sources with an apparent peak flux greater than 1.5 mJy and a signal-to-noise ratio above 30:1) were used for the actual astrometric measurements.

The positions of the sources were determined using the task IMFIT, which fits the sources to an elliptical Gaussian and gives reliable errors based on the postfit residuals between the Gaussian model and the data. IMFIT was used on seven images of smaller areas ( $512 \times 512$  pixel image size) around the pulsar and each background source or group of sources. These images were made and cleaned using MX, with a cell size of  $0''.5$ . We used natural weighting of the data, which gives the best signal-to-noise ratio for a point source, but with somewhat degraded spatial resolution.

A final correction to the positions is necessary before actual astrometric measurements can be made. The motion of the Earth toward or away from the pulsar causes a contraction or expansion of the field of view (caused by the differential yearly aberration across the field of view). The magnification factor is equal to  $1 + v/c$ , where  $v/c$  is the ratio of the component of the Earth's velocity in the direction of the pulsar to the speed of light. The magnification factor was calculated for each epoch and the positions corrected accordingly.

The positions for the pulsar and background sources (labeled BG 1–BG 10) for each observing epoch are given in Table 1 for the equinoxes B1950.0 and J2000.0. The position errors (given in parentheses as the error in the last decimal place) also include a contribution from the error in the position and a nominal error of  $0''.03$  associated with uncertainties in the absolute positional calibration of the VLA. The apparent integrated flux densities (a few of the background sources were slightly extended), separations, and position angles (north through east) from the pulsar are also listed.

<sup>1</sup> Guest User of the NRAO Very Large Array.

<sup>2</sup> The National Radio Astronomy Observatory is operated by Associated Universities, Inc., under a cooperative agreement with the National Science Foundation.

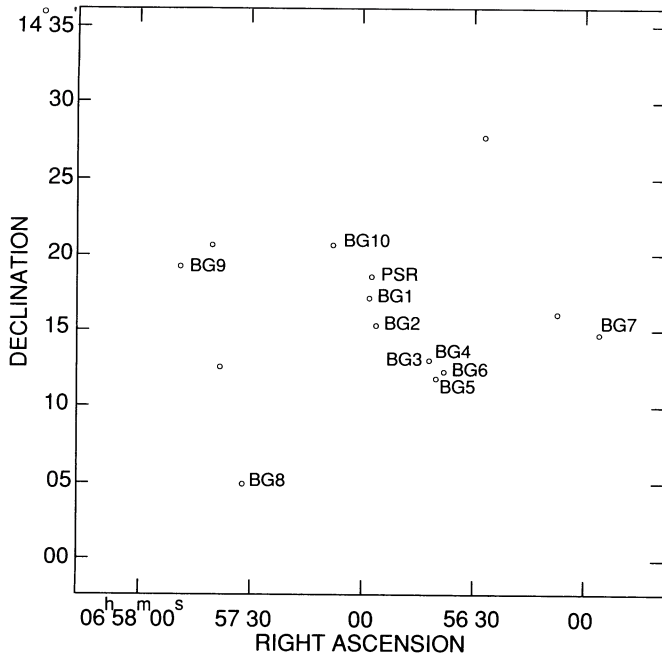


FIG. 1.—Low-resolution image of the entire field of view around PSR 0656 + 14. The open circles show the locations of the pulsar and background sources. See Table 1 for apparent fluxes. Objects not labeled were not sufficiently strong point sources. Sources BG 3 and BG 4 appear as a single unresolved source at low resolution.

## 2. PROPER-MOTION ANALYSIS

Because of the uncertainties in the absolute position calibration of the VLA described above, offsets between the images at different epochs can be as large as  $0''.03$ . Thus, it is generally more accurate to determine the proper motion of an

object from its relative motion with respect to background sources in the field rather than from the change in the measured absolute position of the object between the two epochs. We therefore measured the changes in separation between the pulsar and each BG source from one epoch to the next. As a control on the sensitivity of the experiment, we also calculated the separation between each BG source pair from one epoch to the next. Assuming that these sources are extragalactic objects, each pair separation should be unchanged, within the estimated error.

In Table 2 we have listed the differences in all source pair separations between the two epochs. All of the separations involving background sources are small and are consistent with the error estimate from the IMFIT program. On the other hand, the source-pulsar changes are larger and are consistent with an offset of the pulsar between the two epochs. The somewhat larger differences for all BG 1, BG 9, and BG 10 source pair separations are due to the lower intensities of the sources, as well as the slightly extended nature of BG 1. These three sources are grouped together at the end of Table 2.

The displacement of PSR 0656 + 14 between the two epochs was determined from the average of the 10 entries in Table 2. The final result was taken as the weighted mean of the measurements from each pair. The mean was calculated with the weighting factor equal to  $\sigma^{-2}$ , where  $\sigma$  is the error of the individual measurements. Dividing by the time difference of 1.30 yr gives the proper motion:

$$\mu_{\alpha} = -0''.071 \pm 0''.012 \text{ yr}^{-1},$$

$$\mu_{\delta} = 0''.032 \pm 0''.012 \text{ yr}^{-1},$$

$$\mu = 0''.078 \pm 0''.012 \text{ yr}^{-1},$$

where  $\mu_{\alpha}$  is the motion in right ascension,  $\mu_{\delta}$  is the motion in declination, and  $\mu$  is the overall proper motion. While this is

TABLE 1  
PULSAR AND BACKGROUND SOURCE DATA

SOURCE	B1950		J2000		FLUX (mJy)	SEPARATION	P.A.
	$\alpha$	$\delta$	$\alpha$	$\delta$			
Epoch 1							
PSR .....	06 <sup>h</sup> 56 <sup>m</sup> 57.930(1)	14°18'34".02(1)	06 <sup>h</sup> 59 <sup>m</sup> 48".11	14°14'21".45	6.66	...	...
BG 1 .....	06 56 57.774(2)	14 16 40.63(3)	06 59 47.91	14 12 28.07	2.13	113°.41	181°
BG 2 .....	06 56 56.381(1)	14 15 25.76(2)	06 59 46.49	14 11 13.30	11.12	189.60	187
BG 3 .....	06 56 42.145(3)	14 13 08.05(4)	06 59 32.22	14 08 56.60	15.60	398.61	215
BG 4 .....	06 56 42.276(4)	14 13 04.13(6)	06 59 32.35	14 08 52.67	19.07	400.76	215
BG 5 .....	06 56 40.376(1)	14 12 03.57(1)	06 59 30.43	14 07 52.24	10.20	466.44	213
BG 6 .....	06 56 38.046(1)	14 12 18.92(2)	06 59 28.10	14 08 07.76	3.57	473.54	218
BG 7 .....	06 55 56.159(1)	14 14 46.28(1)	06 58 46.28	14 10 38.07	34.09	926.35	256
BG 8 .....	06 57 32.180(2)	14 05 00.57(3)	07 00 22.07	14 00 45.60	4.53	953.72	149
BG 9 .....	06 57 48.980(3)	14 19 13.89(4)	07 00 39.15	14 14 57.72	2.08	743.15	87
BG 10 .....	06 57 07.951(3)	14 20 45.50(5)	06 59 58.17	14 16 32.22	1.88	196.23	42
Epoch 2							
PSR .....	06 <sup>h</sup> 56 <sup>m</sup> 57.925(2)	14°18'34".10(3)	06 <sup>h</sup> 59 <sup>m</sup> 48".10	14°14'21".53	2.44	...	...
BG 1 .....	06 56 57.758(4)	14 16 40.59(6)	06 59 47.90	14 12 28.03	3.90	113°.53	181°
BG 2 .....	06 56 56.371(2)	14 15 25.83(3)	06 59 46.48	14 11 13.37	9.76	189.62	187
BG 3 .....	06 56 42.136(4)	14 13 08.10(6)	06 59 32.21	14 08 56.65	13.08	398.69	215
BG 4 .....	06 56 42.266(4)	14 13 04.20(7)	06 59 32.34	14 08 52.74	16.30	400.81	215
BG 5 .....	06 56 40.365(1)	14 12 03.60(1)	06 59 30.42	14 07 52.27	8.57	466.53	213
BG 6 .....	06 56 38.035(1)	14 12 18.99(2)	06 59 28.09	14 08 07.83	2.99	473.61	218
BG 7 .....	06 55 56.149(1)	14 14 46.31(1)	06 58 46.27	14 10 38.10	25.40	926.44	256
BG 8 .....	06 57 32.169(2)	14 05 00.73(3)	07 00 22.06	14 00 45.76	5.14	953.60	149
BG 9 .....	06 57 48.962(3)	14 19 13.98(4)	07 00 39.13	14 14 57.81	2.22	742.96	87
BG 10 .....	06 57 07.936(3)	14 20 45.65(5)	06 59 58.15	14 16 32.37	1.53	196.17	42

TABLE 2  
DIFFERENCES IN BACKGROUND SOURCE PAIR  
SEPARATIONS BETWEEN EPOCHS

PAIR	DIFFERENCE	
	$\alpha$	$\delta$
P-BG 1	$-0^{\circ}.16 \pm 0^{\circ}.07$	$0^{\circ}.12 \pm 0^{\circ}.07$
P-BG 2	$-0.07 \pm 0.05$	$0.01 \pm 0.05$
P-BG 3	$-0.06 \pm 0.08$	$0.03 \pm 0.08$
P-BG 4	$-0.07 \pm 0.09$	$0.01 \pm 0.10$
P-BG 5	$-0.09 \pm 0.04$	$0.05 \pm 0.03$
P-BG 6	$-0.09 \pm 0.04$	$0.01 \pm 0.04$
P-BG 7	$-0.07 \pm 0.04$	$0.05 \pm 0.03$
P-BG 8	$-0.09 \pm 0.05$	$0.08 \pm 0.05$
P-BG 9	$-0.19 \pm 0.07$	$0.01 \pm 0.06$
P-BG 10	$-0.15 \pm 0.07$	$0.07 \pm 0.08$
BG 2-BG 3	$0.02 \pm 0.08$	$-0.02 \pm 0.08$
BG 2-BG 4	$0.00 \pm 0.09$	$0.00 \pm 0.10$
BG 2-BG 5	$-0.02 \pm 0.04$	$-0.04 \pm 0.04$
BG 2-BG 6	$-0.02 \pm 0.04$	$0.00 \pm 0.05$
BG 2-BG 7	$0.00 \pm 0.04$	$0.04 \pm 0.04$
BG 2-BG 8	$-0.02 \pm 0.05$	$0.09 \pm 0.06$
BG 3-BG 4	$0.02 \pm 0.11$	$0.02 \pm 0.12$
BG 3-BG 5	$-0.03 \pm 0.08$	$-0.02 \pm 0.07$
BG 3-BG 6	$-0.03 \pm 0.08$	$-0.02 \pm 0.08$
BG 3-BG 7	$0.02 \pm 0.08$	$0.02 \pm 0.07$
BG 3-BG 8	$-0.03 \pm 0.08$	$0.11 \pm 0.08$
BG 4-BG 5	$-0.02 \pm 0.09$	$-0.04 \pm 0.09$
BG 4-BG 6	$-0.02 \pm 0.09$	$0.00 \pm 0.10$
BG 4-BG 7	$0.00 \pm 0.09$	$0.04 \pm 0.09$
BG 4-BG 8	$-0.02 \pm 0.09$	$0.09 \pm 0.10$
BG 5-BG 6	$0.00 \pm 0.03$	$-0.04 \pm 0.03$
BG 5-BG 7	$-0.02 \pm 0.03$	$0.00 \pm 0.02$
BG 5-BG 8	$0.00 \pm 0.05$	$0.13 \pm 0.04$
BG 6-BG 7	$-0.02 \pm 0.03$	$0.04 \pm 0.03$
BG 6-BG 8	$-0.00 \pm 0.05$	$0.09 \pm 0.05$
BG 7-BG 8	$-0.02 \pm 0.05$	$0.13 \pm 0.04$
BG 1-BG 2	$0.09 \pm 0.07$	$0.11 \pm 0.08$
BG 1-BG 3	$0.10 \pm 0.10$	$0.09 \pm 0.10$
BG 1-BG 4	$0.09 \pm 0.11$	$0.11 \pm 0.11$
BG 1-BG 5	$0.07 \pm 0.07$	$0.07 \pm 0.07$
BG 1-BG 6	$0.07 \pm 0.07$	$0.11 \pm 0.07$
BG 1-BG 7	$0.09 \pm 0.07$	$-0.07 \pm 0.07$
BG 1-BG 8	$0.07 \pm 0.08$	$0.20 \pm 0.08$
BG 1-BG 9	$-0.03 \pm 0.09$	$0.13 \pm 0.09$
BG 1-BG 10	$0.02 \pm 0.09$	$-0.19 \pm 0.10$
BG 9-BG 2	$-0.12 \pm 0.07$	$0.02 \pm 0.07$
BG 9-BG 3	$0.13 \pm 0.10$	$-0.04 \pm 0.09$
BG 9-BG 4	$0.12 \pm 0.10$	$-0.02 \pm 0.11$
BG 9-BG 5	$0.10 \pm 0.07$	$-0.06 \pm 0.06$
BG 9-BG 6	$0.10 \pm 0.07$	$0.02 \pm 0.06$
BG 9-BG 7	$-0.12 \pm 0.07$	$0.06 \pm 0.06$
BG 9-BG 8	$0.10 \pm 0.07$	$0.07 \pm 0.07$
BG 10-BG 2	$-0.07 \pm 0.07$	$-0.08 \pm 0.08$
BG 10-BG 3	$-0.09 \pm 0.10$	$-0.10 \pm 0.10$
BG 10-BG 4	$-0.07 \pm 0.10$	$-0.08 \pm 0.12$
BG 10-BG 5	$-0.06 \pm 0.07$	$-0.12 \pm 0.07$
BG 10-BG 6	$-0.06 \pm 0.07$	$-0.08 \pm 0.08$
BG 10-BG 7	$-0.07 \pm 0.07$	$0.12 \pm 0.07$
BG 10-BG 8	$-0.06 \pm 0.07$	$0.01 \pm 0.08$
BG 10-BG 9	$0.04 \pm 0.09$	$-0.06 \pm 0.09$

not an extreme amount of proper motion, it is greater than that of some other well-known pulsars, such as the Vela pulsar (Ögelman, Koch-Miramond, & Aurière 1989; Fomalont et al. 1990).

### 3. PROGENITOR OF MONOGEN RING

In Córdoba et al. (1989), it was shown that the soft X-ray source E0656.9+1418 was, in fact, the radio pulsar PSR

0656+14. As noted in Nousek et al. (1981), the pulsar lies near the geometric center of a ring of soft X-ray emission known as the Gemini-Monoceros X-Ray Enhancement, or Monogem Ring. Two lines of evidence suggested a correlation between the pulsar and the ring. First, the period derivative of the pulsar (Domingue et al. 1986) gives a spin-down age of  $1.1 \times 10^5$  yr; this is comparable to the estimated age of the Monogem Ring of  $6 \times 10^4$  yr (Nousek et al. 1981). Second, Nousek et al. estimate a distance for the ring based on its size, nonthermal radio emission, and neutral hydrogen structure. Their derived limits place the ring between 150 and 500 pc, and they adopt a "characteristic distance" of 300 pc. Córdoba et al. (1989) note that the radio dispersion measure of the pulsar suggests a comparable range of allowed distances to the pulsar.

The proper-motion study described here has yielded additional evidence for a correlation between PSR 0656+14 and the Monogem Ring. Along with the magnitude of proper motion, we have also determined its direction. In the  $\alpha$ - $\delta$  plane of the images, it is in the direction of position angle  $294^\circ$ . The motion of the pulsar is opposite to the direction of the center of the Monogem Ring. In fact, if we retrace the pulsar's proper motion back over the past  $1.1 \times 10^5$  yr, we find that it has traveled  $\sim 2^{\circ}.4 \pm 0^{\circ}.37$  (at a transverse velocity of  $115 \text{ km s}^{-1}$  for an assumed distance of 300 pc) and would have originated at Galactic coordinates  $l = 202^{\circ}.96$ ,  $b = 9^{\circ}.77$ . Figure 2 (Plate L5) shows an improved soft X-ray image of the ring (kindly provided by D. Burrows) with the present position of the pulsar and its direction of motion based on this proper-motion study. The backward extrapolation of the pulsar's motion places it nicely in the central ring area. We caution that the true "center" cannot be determined because the boundary of the ring is not well defined and the ring is slightly asymmetric and is not of uniform intensity. This could be due to many things, e.g., the force of the supernova explosion being asymmetric and the southern portion of the ring colliding with the dust and gas of the Galactic plane. Also, Nousek et al. show that, because of the detector response, even a uniform ring source would not have appeared as such in the X-ray images.

### 4. CONCLUSION

Based on the results of our proper-motion study, the comparable distance and age estimates for the pulsar and the Monogem Ring, and the geometry of the system, it is plausible that the ring is the supernova remnant of the pulsar's progenitor.

This is a potentially important result because PSR 0656+14 may be the compact remnant of the progenitor of the oldest supernova remnant to be detected in association with a pulsar. Detailed analysis of the radio and X-ray properties of the ring and pulsar may provide important information on the late stages of evolution of supernova remnants and the cooling of neutron stars.

Another epoch of 1.385 GHz spectral line mode observations of the pulsar should be made to confirm the magnitude and direction of the proper motion reported here. This is especially important because most of the background sources strong enough to be used for relative positions are on one side of the pulsar.

We acknowledge partial support for this work from the US Department of Energy and Los Alamos National Laboratory's Institute for Geophysics and Planetary Physics.

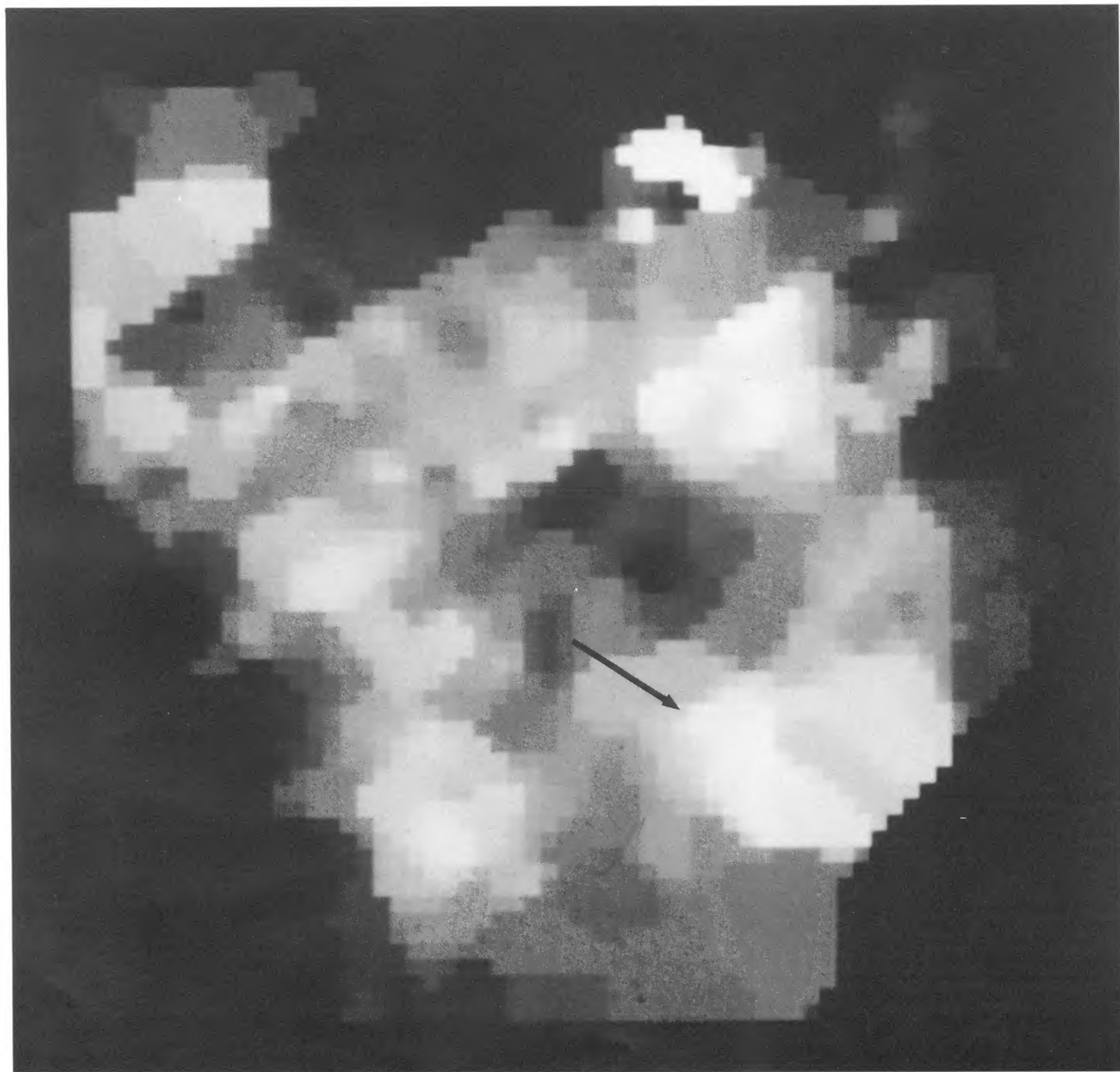


FIG. 2.—X-ray  $\frac{1}{4}$  keV intensity plot of the Monogem ring; this is a refinement of the figure presented in Nousek et al. (1981). The pixel size is  $1^\circ \times 1^\circ$ . The head of the arrow shows the current position of the pulsar, and the length shows the extent and direction of the pulsar's proper motion over the past  $1.1 \times 10^5$  yr. Note: Neither the bright spot at top center in the figure (which is U Gem in outburst) nor the bright feature at top left is associated with the ring.

THOMPSON ET AL. (see 366, L85)

## REFERENCES

- Córdova, F. A., Hjellming, R. M., Mason, K. O., & Middleditch, J. 1989, ApJ, 345, 451  
Domingue, D., Rankin, J. M., Weisberg, J. M., & Backus, P. R. 1986, A&A, 161, 303  
Fomalont, E. B., Goss, W. M., Lyne, A. G., & Manchester, R. N. 1990, preprint  
Nousek, J. A., Cowie, L. L., Hu, E., Lindblad, C. J., & Garmire, G. P. 1981, ApJ, 248, 152  
Ögelman, H., Koch-Miramond, L., & Aurière, M. 1989, preprint